International Journal of Mechanical Sciences 96-97 (2015) 132–142

Contents lists available at ScienceDirect

International Journal of Mechanical Sciences

journal homepage: www.elsevier.com/locate/ijmecsci

Nonlocal mass-nanosensor model based on the damped vibration of single-layer graphene sheet influenced by in-plane magnetic field

Danilo Karličić [a], Predrag Kozić [a], Sondipon Adhikari [b], Milan Cajić [c], Tony Murmu [d,*], Mihailo Lazarević [e]

[a] Faculty of Mechanical Engineering, University of Niš, A. Medvedeva 14, 18000 Niš, Serbia
[b] College of Engineering, Swansea University, Singleton Park, Swansea SA2 8PP, UK
[c] Mathematical Institute, Serbian Academy of Sciences and Arts, Kneza Mihaila 36, 11001 Belgrade, Serbia
[d] School of Engineering, University of the West of Scotland, Paisley PA12BE, UK
[e] Faculty of Mechanical Engineering, University of Belgrade, Kraljice Marije 16, 11000 Belgrade, Serbia

ARTICLE INFO

Article history:
Received 25 November 2014
Received in revised form
3 March 2015
Accepted 19 March 2015
Available online 28 March 2015

Keywords:
Nonlocal elasticity theory
Mass-nanosensor
In-plane magnetic field
Damped natural frequency
Damped frequency shift

ABSTRACT

Nano-materials such as graphene sheets have a great opportunity to be applied in development of a new generation of nanomechanical sensors and devices due to their unique physical properties. Based on the nonlocal continuum theory and vibration analysis, the single-layered graphene sheet with attached nanoparticles affected by in-plane magnetic field is proposed as a new type of the mass-nanosensor. The nonlocal Kirchhoff-Love plate theory is adopted to describe mechanical behavior of single-layered graphene sheet as an orthotropic nanoplate. The equation of motion of a simply supported orthotropic nanoplate is derived, where the influence of Lorentz magnetic force is introduced through classical Maxwell's equations. Complex natural frequencies, damped frequency shifts and relative shift of damping ratio for nanoplate with attached nanoparticles are obtained in the explicit form. The influences of the nonlocal and magnetic field parameter, different mass weights and positions of attached nanoparticles and damping coefficients on the relative damped frequency shift and relative shift of damping ratio are examined. The presented results can be useful in the analysis and design of nanosensors applied in the presence of strong magnetic field. Our results show that magnetic field could be successfully used to improve sensibility performances of nanomechanical sensors.

1. Introduction

Recent developments of nanomechanical sensors cause an increase of a number of theoretical studies constructing the mathematical framework to investigate their dynamic behavior and performances. This can be especially important in predesign procedures of mass-sensor devices. In the literature, one can find many examples of application of nanomechanical sensors for calorimetric gas detection, drug screening, genetics, proteomics, glycemic, microbiology, metabolic measurements and other applications in chemical, environmental and biological detection [1,2]. In some of the works, graphene sheet nanostructures are suggested for nanosensor application where one of the advantages compared to the CNT based sensors is the larger surface for catching the particles. In the following, we give a short review of scientific works where molecular dynamics and nonlocal continuum methods are applied to examine mass-nanosensors. In the work by Sakhaee-Pour et al. [3], the authors have investigated the application of single-layer graphene sheet as strain sensor by using the molecular structural mechanics approach. For the first time, a closed-form equation for the frequency shift caused by added mass on carbon nanotube sensor was derived in [4] using the energy principles. The authors also investigated the linear approximation of the nonlinear sensor equation and validated the results for a wide range of cases. Adhikari and Chowdhury [5] derived closed-form transcendental equations for the frequency shift from added point and distributed mass by using the energy principles. In addition, the authors calculated the calibration constants proposed in order to obtain explicit relations between the added mass and frequency shift. Further, in [6] the same authors proposed a single-layer graphene sheet as mass sensor. By developing the appropriate mathematical framework, they considered four types of distributed mass loadings, obtained explicit relations between frequency shift and added mass as well as for non-dimensional calibration constants. The obtained results are validated with molecular dynamics simulation. In the

* Corresponding author. Tel.: +44 141 848 3235.
E-mail address: murmutony@gmail.com (T. Murmu).

http://dx.doi.org/10.1016/j.ijmecsci.2015.03.014
0020-7403/

previously described papers, classical continuum or molecular dynamics models are used to describe the dynamic behavior of nanostructures.

It is well known that better results in describing the dynamics behavior of nanostructures can be achieved by using the nonlocal continuum models based on nonlocal theory of Eringen [7,8]. Such models are widely used in the literature to describe various dynamics and stability behaviors of nanorods, nanobeams, nanoplates and shell-like nanostructures [9–19]. By taking into account size-dependent nonlocal parameter into a nonlocal constitutive relation, we consider nonlocal inter-atomic forces that cannot be neglected at nano-scale level. Thus, when using the nonlocal models, obtained frequencies and frequency shifts due to an added mass for nanosensing application should be more accurate. The value of nonlocal parameter is usually obtained by fitting the results from molecular dynamics simulation where typical values for nanobeams and nanoplates can be found in the literature. Murmu and Adhikari [20] proposed a nonlocal elasticity modeling approach for CNT based cantilever mass-sensor. They obtained explicit equations for calibration constants and frequency shifts by adding point and distributed masses. They also validated the obtained results with the results from molecular dynamics simulation. On the example of multiple strands of deoxythimidine attached on CNT, they showed the advantage of nonlocal elasticity approach comparing to the local one. Recently, in [21] the same authors suggest single-layer graphene sheet (SLGS) as nano-scale mass sensor where graphene is modeled as an isotropic nanoplate by using the nonlocal elasticity theory. In this case, they also obtained closed-form expressions for the frequency shifts caused by attached masses as well as for calibration constants by applying the energy principles. From numerical results they reviled that the sensitivity of nanosensors is in the order of gigahertz i.e. zeptogram. Shen et al. [22] applied nonlocal Kirchhoff plate theory to model nanomechanical sensor based on SLGS. The authors obtained natural frequencies using the Galerkin method and investigated the frequency shifts and nanosensor performances for different locations of attached masses and changes of the nanoplate dimensions. Vibration of CNT mass-sensors incorporating the thermal and nonlocal effects was investigated by Wang and Wang [23]. In addition, Fazalzadeh and Ghavanloo [24] examined the vibration of SLGS for mass sensing application also incorporating the nonlocal and thermal effects. Kiani [25] studied the specific and interesting problem of vibration of single-walled carbon nanotube (SWCNT) under the influence of axial magnetic field used for mass sensing application. The author obtained explicit expressions for the frequency shift of magnetically affected SWCNTS caused by addition of nanoparticles. In [46,48–50] the same author analyzed the vibration behaviors of single/double-walled carbon nanotubes and graphene sheet subjected to the magnetic field in different directions with respect to these nanostructures.

Nonlocal damped vibrations of various nanostructures are investigated successfully in the literature by using different nonlocal viscoelastic constitutive relations [26–30]. The main property of systems with damping is dissipation of a total mechanical energy of the system. Moreover, studying the sources of damping is a crucial point in the analysis of a dynamical behavior of nano-electromechanical systems (NEMS) such as nanoresonators, nanoactuators and also bio/mass sensors etc. [31]. By searching the literature, one can notice that the earlier authors have defined two types of damping sources in dynamical systems: I) external damping from the influence of the surrounding media [27] and II) internal damping or the so-called material damping which comes from constitutive relations [29,30]. Croy et al. [32], proposed graphene based nanoresonators with nonlinear damping effects using the continuum mechanical model. The authors have found that the coupling between flexural modes and in-plane phonons leads to linear and nonlinear damping for out of-plane vibration. Further, Eichler et al. [33] studied damping effects in mechanical resonators based on carbon nanomaterials such a graphene sheets and carbon nanotubes. They showed the influence of different values of damping coefficient on the dynamical behavior of mechanical nanoresonators, where damping strongly depends on the amplitude of motion that was described by the nonlinear damping force. Karličić et al. [34] investigated the free damped vibration of the system of multiple graphene sheets embedded in viscoelastic medium. They obtained closed form solutions for complex natural frequencies and found asymptotical values of natural frequencies and damping ratios of such a system. Alibeigloo [51] employed nonlocal and three-dimensional elasticity theory to examine the vibration properties of nanoplate. The author examined the effects of non-local parameter, aspect ratio, thickness-to-length ratio and half-wave numbers on the frequency behavior. It was found that length-to-thickness ratio significantly influences the vibration behavior of graphene i.e. the frequency increases significantly for ratio in the range 5–20 and for higher aspect ratios these changes are minimal. Further, the author revealed that nonlocal parameter is almost independent of the length-to-thickness ratio.

Besides previously mentioned models of single layer graphene sheets (SLGS) based on molecular structural mechanics approach or continuum theory, in the literature one can find other approaches based on molecular dynamics that accounts for the effects depending on anisotropy and chirality of graphene. Liu et al. [52] investigated the buckling behavior of graphene under compression strain. The authors have found that different buckling behaviors can be expected for different width-to-length aspect ratios and chirality of graphene. Further, the authors linked sudden changes of buckling behavior for certain ranges of aspect ratio to the presence of edge effects in graphene. In the end, they came to the conclusion that after certain value of aspect ratio all mentioned non-continuum effect can be neglected. In [53], Liu et al. analyzed the transverse wave propagation in single-layer graphene sheet using molecular dynamics simulation and continuum analysis. The authors found that there is an upper limit of the excitation frequency under which wave propagation is distorted. In addition, they have shown that for certain frequency range transverse wave propagation in graphene significantly depends on chirality.

In spite of many published results in the field of damped vibration of nanostructures and nanomechanical sensors, there are no studies analyzing the damping effect on resonant frequencies of graphene based nanosensors affected by magnetic field. In this paper, we present a novel theoretical approach to examine the properties of mass-nanosensors based on SLGS by using the nonlocal plate theory, considering the internal damping and external damping from viscoelastic medium and taking into account the effect of in-plane magnetic field. Motion equations of the system are derived applying the Lorentz force and Maxwell equations for the magnetic field. Closed-form solutions for relative damped frequency shifts and relative damped ratio shifts due to added masses are obtained. Performances of the mass-nanosensor are investigated for different positions of masses, mass weights and changes of magnetic field and viscoelastic parameters. Since the effect of thickness-to-length ratio play an important role in the mechanical behavior of graphene sheets, we also examined its influence on mass-nanosensor. We have shown that this parameter can be very important in a selection of optimal dimension of graphene sheet to achieve the best sensitivity of nanosensor device. In addition, our results illustrate that the presence of magnetic field could successfully improve the sensibility performances of nanomechanical sensors.

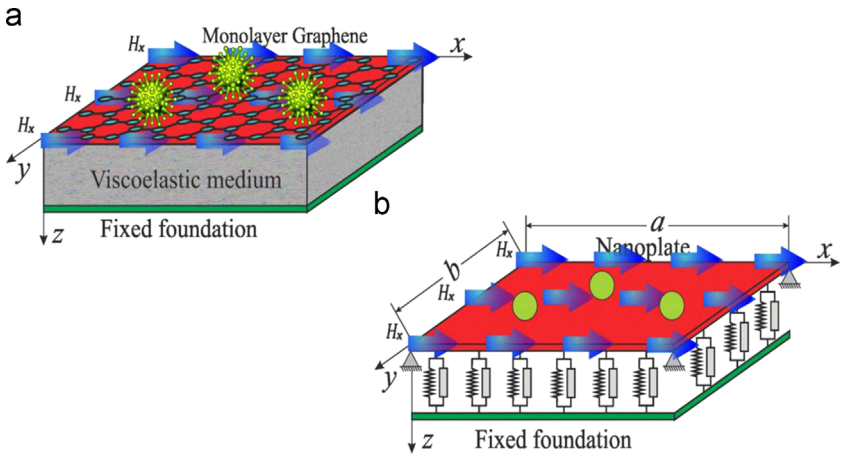

Fig. 1. Single-layered graphene sheet as mass-nanosensors with attached nanoparticles: (a) physical model and (b) mechanical model.

2. Nonlocal model of graphene bio-sensor

In this study, we proposed Kirchhoff-Love theory for orthotropic nanoplate to describe mechanical behavior of single-layered graphene sheet Fig. 1a) with attached nanoparticles such as viruses or biomolecules, based on the nonlocal viscoelastic constitutive relation. Further, it is assumed that some types of viruses and biomolecules or nanoparticles can be modeled as mass points because of their small dimensions compared to the dimension of a nanoplate. This implies that we can ignore influence of the rotational inertia of attached nanoparticles as proposed in the literature [4,6,20,21].

It should be noted that we assume that attached nanoparticles are perfectly rigidly attached to the nanoplate without considering van der Walls interaction forces. This leads to the fact that there is no separation of nanoparticles from the graphene sheet during motion. Moreover, there is no additional interaction among attached nanoparticles since the distance is large enough and in the literature [4–6,23–25,43]. In [4–6,21], it is found that the results obtained by nonlocal continuum mechanics approach and molecular dynamic simulation are in good agreement. In these works, the influences of transversal displacements of nanoparticles and van der Waals forces between nanoparticles and graphene sheet have been neglected.

Consider the continuum mechanical model (see Fig. 1b)) of such mass-nanosensors is represented by an orthotropic nanoplate with the following material properties: elastic modulus E_1 and E_2, Poison coefficients ϑ_{12} and ϑ_{21}, shear modulus G_{12}, internal damping parameter τ_d, mass density ρ, length a, width b and thickness h. Further, we assume that the orthotropic nanoplate is resting on the viscoelastic medium, which is modeled with continuously distributed pairs of springs and dampers, also known as Kelvin–Voigt model, where stiffness coefficients is denoted with $\tilde{k}$ and damping coefficients with $\tilde{b}$. Also, we consider that a nanoplate is under the influence of in-plane magnetic field along direction of O–x axes. The x-coordinate is taken along the length of the nanoplate, the y-coordinate along the width of the nanoplate and the z-coordinate is along the thickness of the nanoplate. It should be noted that the flexural vibration of the nanoplate in the thickness direction and transversal displacements are denoted by $w(x,y,t)$.

2.1. Constitutive relations

Now, we will consider the basic equation of nonlocal elasticity and viscoelasticity in the general and two-dimensional case. Eringen and Edelen [7] derived a constitutive relation for nonlocal stress tensor at a point $\boldsymbol{x}$ in an integral form based on the assumption that the stress at a point is a function of the strains at all points of elastic body. Fundamental form of the nonlocal elastic constitutive relation for a three-dimensional linear, homogeneous isotropic body is expressed as:

$$\sigma_{ij}(\boldsymbol{x}) = \int \alpha(|\boldsymbol{x}-\boldsymbol{x}'|,\tau) C_{ijkl}\varepsilon_{kl}(\boldsymbol{x}')dV(\boldsymbol{x}'), \forall \boldsymbol{x} \in V, \tag{1a}$$

$$\sigma_{ij,j} = 0, \tag{1b}$$

$$\varepsilon_{ij} = \frac{1}{2}(u_{i,j}+u_{j,i}), \tag{1c}$$

where C_{ijkl} is the elastic modulus tensor for classical isotropic elasticity; σ_{ij} and ε_{ij} are the stress and the strain tensors, respectively, and u_i is the displacement vector. With $\alpha(|x-x'|,\tau)$ we denote the nonlocal modulus or attenuation function, which incorporates nonlocal effects into the constitutive equation at a reference point x produced by the local strain at a source x'. The above absolute value of the difference $|x-x'|$ denotes the Euclidean metric. The parameter τ is equal to $\tau = (e_0\tilde{a})/l$ where l is the external characteristic length (crack length, wave length), $\tilde{a}$ describes the internal characteristic length (granular size, distance between C–C bounds, lattice parameter) and e_0 is a constant appropriate to each material that can be identified from atomistic simulations or by using the dispersive curve of the Born–Karman model of lattice dynamics.

Because of difficulties arising in the analytical analysis of continuum systems due to the integral form of nonlocal constitutive equations, Eringen [8] has reformulated them into a differential form. Such form of nonlocal constitutive equations is proved to be very efficient, simple, and convenient for analytical techniques of solving the problems in vibration analysis of nanostructured systems. The differential form of the nonlocal constitutive relation is:

$$(1-\mu\nabla^2)\sigma_{ij} = t_{ij}, \tag{2}$$

where $\nabla^2 = (\partial^2/\partial x^2)+(\partial^2/\partial y^2)$ is the Laplacian; $\mu = (e_0\tilde{a})^2$ is the nonlocal parameter; and $t_{ij} = C_{ijkl}\varepsilon_{kl}$ is the classical stress tensor. From Eq. (2), the constitutive relations for homogeneous elastic nanoplates can be expressed as:

$$(1-\mu\,\nabla^2)\begin{pmatrix}\sigma_{xx}\\ \sigma_{yy}\\ \tau_{xy}\end{pmatrix} = \begin{bmatrix}\frac{E}{1-\vartheta^2} & \frac{\vartheta E}{1-\vartheta^2} & 0\\ \frac{\vartheta E}{1-\vartheta^2} & \frac{E}{1-\vartheta^2} & 0\\ 0 & 0 & G\end{bmatrix}\begin{pmatrix}\varepsilon_{xx}\\ \varepsilon_{yy}\\ \gamma_{xy}\end{pmatrix}, \tag{3}$$

where E, G and ϑ are the Young's modulus, shear modulus and Poisson's ratio, respectively.

The nonlocal viscoelastic constitutive relation for Kelvin–Voigt viscoelastic nanoplate proposed by Pouresmaeeli et al. [29] and Karličić et al. [34] is a combination of nonlocal elasticity and viscoelasticity theory. For the case of two-dimensional nonlocal viscoelastic orthotropic nanoplate, constitutive relation is given as:

$$(1-\mu\nabla^2)\begin{pmatrix}\sigma_{xx}\\ \sigma_{yy}\\ \tau_{xy}\end{pmatrix}=\begin{bmatrix}\frac{E_1(1+\tau_d\frac{\partial}{\partial t})}{1-\vartheta_{12}\vartheta_{21}} & \frac{\vartheta_{12}E_1(1+\tau_d\frac{\partial}{\partial t})}{1-\vartheta_{12}\vartheta_{21}} & 0\\ \frac{\vartheta_{12}E_2(1+\tau_d\frac{\partial}{\partial t})}{1-\vartheta_{12}\vartheta_{21}} & \frac{E_2(1+\tau_d\frac{\partial}{\partial t})}{1-\vartheta_{12}\vartheta_{21}} & 0\\ 0 & 0 & G_{12}(1+\tau_d\frac{\partial}{\partial t})\end{bmatrix}\begin{pmatrix}\varepsilon_{xx}\\ \varepsilon_{yy}\\ \gamma_{xy}\end{pmatrix} \tag{4}$$

where τ_d is the internal damping coefficient of nanoplate, E_1, E_2 and ϑ_{12}, ϑ_{21} are Young's modulus's and Poisson's ratios of orthotropic nanoplate. By neglecting the internal viscosity i.e. for $\tau_d=0$, we then obtain the constitutive relation of nonlocal elasticity. In the follow, we use the constitutive relation for nonlocal viscoelasticity in Eq. (4) to derive governing equations of motion.

2.2. Classical Maxwell's relation

On the basis of the classical Maxwell relation [35–42], the relationships between the current density $\mathbf{J}$, distributing vector of magnetic field $\mathbf{h}$, strength vectors of the electric fields $\mathbf{e}$ and magnetic field permeability η are represented by Maxwell's equations in differential form and can be retrieved as:

$$\mathbf{J}=\nabla\times\mathbf{h},\quad \nabla\times\mathbf{e}=-\eta\frac{\partial\mathbf{h}}{\partial t},\quad \nabla\cdot\mathbf{h}=0, \tag{5}$$

where vectors of distributing magnetic field $\mathbf{h}$ and the electric field $\mathbf{e}$ are defined as:

$$\mathbf{h}=\nabla\times(\mathbf{U}\times\mathbf{H}),\quad \mathbf{e}=-\eta\left(\frac{\partial\mathbf{U}}{\partial t}\times\mathbf{H}\right). \tag{6}$$

In the above equation, $\nabla=(\partial/\partial x)\mathbf{i}+(\partial/\partial y)\mathbf{j}+(\partial/\partial z)\mathbf{k}$ is the Hamilton operator, $\mathbf{U}(x,y,z)=\overline{u}_x\mathbf{i}+\overline{v}_y\mathbf{j}+\overline{w}_z k$ is the displacement vector and $\mathbf{H}=(H_x,0,0)$ is the vector of the in-plane magnetic field. It is assumed that the in-plane magnetic field acts on the orthotropic viscoelastic nanoplate in the x-direction. We can write the vector of the distributing magnetic field in the following form:

$$\mathbf{h}=-H_x\left(\frac{\partial\overline{v}_y}{\partial y}+\frac{\partial\overline{w}_z}{\partial z}\right)\mathbf{i}+H_x\frac{\partial\overline{v}_y}{\partial x}\mathbf{j}+H_x\frac{\partial\overline{w}_z}{\partial x}\mathbf{k}. \tag{7}$$

Introducing Eq. (7) to the first expressions of Eq. (5) one obtains:

$$\begin{aligned}\mathbf{J}=\nabla\times\mathbf{h}=H_x\left(-\frac{\partial^2\overline{v}_y}{\partial x\partial z}+\frac{\partial^2\overline{w}_z}{\partial x\partial y}\right)\mathbf{i}-H_x\left(\frac{\partial^2\overline{v}_y}{\partial y\partial z}+\frac{\partial^2\overline{w}_z}{\partial x^2}+\frac{\partial^2\overline{w}_z}{\partial z^2}\right)\mathbf{j}\\ +H_x\left(\frac{\partial^2\overline{v}_y}{\partial x^2}+\frac{\partial^2\overline{v}_y}{\partial y^2}+\frac{\partial^2\overline{w}_z}{\partial z\partial y}\right)\mathbf{k}.\end{aligned} \tag{8}$$

Further, using Eq. (8) into the expressions for the Lorentz force induced by the in-plane uniaxial magnetic field, yields:

$$\begin{aligned}\mathbf{f}\left(f_x,f_y,f_z\right)=\eta(\mathbf{J}\times\mathbf{H})=\eta\Bigg[0\mathbf{i}+H_x^2\left(\frac{\partial^2\overline{v}_y}{\partial x^2}+\frac{\partial^2\overline{v}_y}{\partial y^2}+\frac{\partial^2\overline{w}_z}{\partial z\partial y}\right)\mathbf{j}\\ +H_x^2\left(\frac{\partial^2\overline{w}_z}{\partial x^2}+\frac{\partial^2\overline{w}_z}{\partial z^2}+\frac{\partial^2\overline{v}_y}{\partial z\partial y}\right)\mathbf{k}\Bigg].\end{aligned} \tag{9}$$

here f_x,f_y and f_z are the Lorentz forces along the x, y and z directions, respectively of the form

$$f_x=0, \tag{10a}$$

$$f_y=\eta H_x^2\left(\frac{\partial^2\overline{v}_y}{\partial x^2}+\frac{\partial^2\overline{v}_y}{\partial y^2}+\frac{\partial^2\overline{w}_z}{\partial z\partial y}\right), \tag{10b}$$

$$f_z=\eta H_x^2\left(\frac{\partial^2\overline{w}_z}{\partial x^2}+\frac{\partial^2\overline{w}_z}{\partial z^2}+\frac{\partial^2\overline{v}_y}{\partial z\partial y}\right). \tag{10c}$$

In this study, we assume that the displacement of the orthotropic viscoelastic nanoplate $\overline{w}_z(x,y,t)$ and the Lorentz force acts only in z direction that can be written as:

$$f_z=\eta H_x^2\left(\frac{\partial^2\overline{w}_z}{\partial x^2}+\frac{\partial^2\overline{w}_z}{\partial z^2}+\frac{\partial^2\overline{v}_y}{\partial z\partial y}\right). \tag{11}$$

Now, it is possible to obtain the transverse Lorentz magnetic force [46–50], which acts on the orthotropic viscoelastic nanoplate with the corresponding displacement field for Kirchhoff-Love plate theory given as:

$$\tilde{q}(x,y,t)=\int_{-h/2}^{h/2}f_z dz=\eta h H_x^2\left(\frac{\partial^2 w}{\partial x^2}-\frac{\partial^2 w}{\partial y^2}\right), \tag{12}$$

where the bending moments of that force are equal to zero $\overline{M}(x,y,t)=\int_{-h/2}^{h/2}zf_z dz=0$.

2.3. The nonlocal Kirchhoff-Love plate theory

The displacement field of the Kirchhoff-Love plate theory in x, y and z directions is given as:

$$\overline{u}_x=u(x,y,t)-z\frac{\partial w(x,y,t)}{\partial x},\ \overline{v}_y=v-z\frac{\partial w(x,y,t)}{\partial y},\ \overline{w}_z=w(x,y,t), \tag{13}$$

in which u, v and w are the displacements of orthotropic nanoplates in the x,y and z directions, respectively. For given displacement field Eq. (13), the nonzero strain–displacement relations are:

$$\varepsilon_{xx}=\frac{\partial u}{\partial x}-z\frac{\partial^2 w}{\partial x^2},\ \varepsilon_{yy}=\frac{\partial v}{\partial x}-z\frac{\partial^2 w}{\partial y^2},\ \gamma_{xy}=\frac{\partial u}{\partial y}+\frac{\partial v}{\partial x}-2z\frac{\partial^2 w}{\partial x\partial y}, \tag{14}$$

where ε_{xx}, and ε_{yy} are the normal strains, and γ_{xy} is the shear strain. According to Newton's second law, equilibrium equations for infinitesimal element can be obtained as:

$$q+\frac{\partial Q_x}{\partial x}+\frac{\partial Q_y}{\partial y}=\rho h\frac{\partial^2 w}{\partial t^2}, \tag{15a}$$

$$\frac{\partial M_{xx}}{\partial x}+\frac{\partial M_{xy}}{\partial y}=Q_x, \tag{15b}$$

$$\frac{\partial M_{yy}}{\partial y}+\frac{\partial M_{xy}}{\partial x}=Q_y, \tag{15c}$$

$$\frac{\partial N_{xx}}{\partial x}+\frac{\partial N_{xy}}{\partial y}=\rho h\frac{\partial^2 u}{\partial t^2}, \tag{15d}$$

$$\frac{\partial N_{yy}}{\partial y}+\frac{\partial N_{xy}}{\partial x}=\rho h\frac{\partial^2 v}{\partial t^2}, \tag{15e}$$

where q is external load represented as a sum of attached masses, in-plane magnetic field and viscoelastic foundation in the following form

$$\begin{aligned}q(x,y,t)=-\tilde{k}w-\tilde{b}\dot{w}+\eta h H_x^2\left(\frac{\partial^2 w}{\partial x^2}-\frac{\partial^2 w}{\partial y^2}\right)\\ -\left(\sum_{j=1}^{s}m_j\delta\left(x-x_j,y-y_j\right)\right)\frac{\partial^2 w}{\partial t^2},\end{aligned} \tag{16}$$

where m_j is the mass of jth attached nanoparticle and $\delta\left(x-x_j,y-y_j\right)$ is the Dirac delta function in two-dimensional case. The terms N_{xx}, N_{yy} and N_{xy} are the in-plane stress resultants M_x, M_y and M_{xy} are the moment resultants, and Q_x and Q_y are the transverse shearing resultants, which are defined as:

$$\begin{aligned}(N_{xx},N_{yy},N_{xy}M_x,M_y,M_{xy},Q_x,Q_y)=\int_{-h/2}^{h/2}(\sigma_{xx},\sigma_{yy},\tau_{xy},z\sigma_{xx},\\ z\sigma_{yy},z\tau_{xy},\ \tau_{xz},\tau_{yz})dz.\end{aligned} \tag{17}$$

By substituting Eqs. (15b) and (15c) into Eq. (15a) and neglecting the in-plane displacements u and v, we obtain the following

partial differential equation of motion for the orthotropic nanoplate as:

$$\frac{\partial^2 M_{xx}}{\partial x^2}+\frac{\partial^2 M_{yy}}{\partial y^2}+2\frac{\partial^2 M_{xy}}{\partial x\partial y}=\rho h\frac{\partial^2 w}{\partial t^2}+\tilde{k}w+\tilde{b}\dot{w}-\eta h H_x^2\left(\frac{\partial^2 w}{\partial x^2}-\frac{\partial^2 w}{\partial y^2}\right)+\left(\sum_{j=1}^{s} m_j\delta\left(x-x_j,y-y_j\right)\right)\frac{\partial^2 w}{\partial t^2}, \tag{18}$$

Now, inserting the strain–displacement relations Eq. (14) into Eq. (4) and using Eqs. (16) and (17), yields

$$(1-\mu\,\Delta)M_{xx}=-D_{11}\left(1+\tau_d\frac{\partial}{\partial t}\right)\frac{\partial^2 w}{\partial x^2}-D_{12}\left(1+\tau_d\frac{\partial}{\partial t}\right)\frac{\partial^2 w}{\partial y^2}, \tag{19a}$$

$$(1-\mu\,\Delta)M_{yy}=-D_{12}\left(1+\tau_d\frac{\partial}{\partial t}\right)\frac{\partial^2 w}{\partial x^2}-D_{22}\left(1+\tau_d\frac{\partial}{\partial t}\right)\frac{\partial^2 w}{\partial y^2}, \tag{19b}$$

$$(1-\mu\,\Delta)M_{xy}=-2D_{66}\left(1+\tau_d\frac{\partial}{\partial t}\right)\frac{\partial^2 w}{\partial x\partial y}, \tag{19c}$$

in which D_{11}, D_{12}, D_{22} and D_{66} are the bending rigidities of orthotropic viscoelastic nanoplates which are expressed as:

$$D_{11}=\frac{E_1h^3}{12(1-\vartheta_{12}\vartheta_{21})},\quad D_{12}=\frac{\vartheta_{12}E_2h^3}{12(1-\vartheta_{12}\vartheta_{21})},$$
$$D_{22}=\frac{E_2h^3}{12(1-\vartheta_{12}\vartheta_{21})},\quad D_{66}=\frac{G_{12}h^3}{12}. \tag{20}$$

The governing equation of motion of viscoelastic orthotropic nanoplate with attached masses in strong magnetic field can be obtain in terms of transversal displacement by using Eqs. (18)–(20), in the following form

$$\begin{aligned}&\rho h\frac{\partial^2 w}{\partial t^2}+\tilde{k}w+\tilde{b}\dot{w}-\eta h H_x^2\left(\frac{\partial^2 w}{\partial x^2}-\frac{\partial^2 w}{\partial y^2}\right)+\left(\sum_{j=1}^{s} m_j\delta\left(x-x_j,y-y_j\right)\right)\frac{\partial^2 w}{\partial t^2}\\&+D_{11}\left(1+\tau_d\frac{\partial}{\partial t}\right)\frac{\partial^4 w}{\partial x^4}+D_{22}\left(1+\tau_d\frac{\partial}{\partial t}\right)\frac{\partial^4 w}{\partial y^4}\\&+2(D_{12}+2D_{66})\left(1+\tau_d\frac{\partial}{\partial t}\right)\frac{\partial^2 w}{\partial x^2\partial y^2}\\&=\mu\left(\frac{\partial^2}{\partial x^2}+\frac{\partial^2}{\partial y^2}\right)\left[\rho h\frac{\partial^2 w}{\partial t^2}+\tilde{k}w+\tilde{b}\dot{w}-\eta h H_x^2\left(\frac{\partial^2 w}{\partial x^2}-\frac{\partial^2 w}{\partial y^2}\right)+\left(\sum_{j=1}^{s} m_j\delta\left(x-x_j,y-y_j\right)\right)\frac{\partial^2 w}{\partial t^2}\right],\end{aligned} \tag{21}$$

and corresponding boundary condition for simply supported nanoplates defined as

$$w(x,0,t)=w(x,b,t)=0,\quad w(0,y,t)=w(a,y,t)=0, \tag{22a}$$

$$M_{xx}(0,y,t)=M_{xx}(a,y,t)=0,\quad M_{yy}(x,0,t)=M_{yy}(x,b,t)=0. \tag{22b}$$

From a physical point of view, this means that the deflections and moments at all four edges of nanoplates are equal to zero.

3. Vibrational response of SLGS with attached nanoparticles

In order to obtain analytical solution for damped natural frequency, damping ratio and damped shift frequency, we assume the solution of partial differential Eq. (21) with corresponding boundary conditions (22) in the following form

$$w(x,y,t)=\sum_{r=1}^{\infty}\sum_{n=1}^{\infty}W_{rn}\,\sin(\alpha_r x)\sin(\beta_n y)e^{i\Omega_{rn}\tau},\ (r,n)=1,2,3,..,\infty, \tag{23}$$

where $i=\sqrt{-1}$, $\alpha_r=r\pi/a$; $\beta_n=n\pi/b$ $(r,n=1,2,3,..,\infty)$; W_{rn} and Ω_{rn} are amplitudes and complex natural frequencies, respectively. According to the paper presented by Karličić et al. [34], the assumed displacement field satisfies the given boundary conditions and it is independent of the influence of viscoelastic interaction. Introducing assumed solution (23) into partial differential equation of motion (21), multiplying both sides of obtained equation with mode shape function $\sin(\alpha_r x)\sin(\beta_n y)$ and integrating over the whole domain yields the following quadratic equation:

$$-\Omega_{rn}^2\tilde{A}+i\Omega_{rn}\tilde{B}+\tilde{C}=0, \tag{24a}$$

in which

$$\tilde{A}=\Lambda\left[\rho h+\sum_{j=1}^{s}\frac{4m_j}{ab}\sin^2(\alpha_r x_j)\sin^2\left(\beta_n y_j\right)\right], \tag{24b}$$

$$\tilde{B}=\tilde{b}\Lambda+\tau_d\left(\alpha_r^4D_{11}+\beta_n^4D_{22}+2\alpha_r^2\beta_n^2(D_{12}+2D_{66})\right), \tag{24c}$$

$$\tilde{C}=\tilde{k}\Lambda+\eta h H_x^2\left(\alpha_r^2-\beta_n^2\right)\Lambda+\alpha_r^4D_{11}+\beta_n^4D_{22}+2\alpha_r^2\beta_n^2(D_{12}+2D_{66}), \tag{24d}$$

$$\Lambda=1+\mu\left(\alpha_r^2+\beta_n^2\right), \tag{24e}$$

are constants, where we use orthogonality condition and property of Dirac delta function in the form

$$\int_0^a\int_0^b \sin\frac{r\pi}{a}x\,\sin\frac{n\pi}{b}y\,\sin\frac{s\pi}{a}x\,\sin\frac{m\pi}{b}y\,dxdy=\begin{cases}\frac{ab}{4}, & rn=sm\\ 0, & rn\neq sm\end{cases} \tag{25a}$$

and

$$\delta\left(x-x_j,y-y_j\right)=0\ \text{if}(x,y)\neq\left(x_j,y_j\right),\quad \text{and}$$
$$\int_{-\infty}^{\infty}\int_{-\infty}^{\infty}\delta\left(x-x_j,y-y_j\right)dxdy=1. \tag{25b}$$

By solving the quadratic equation expressed in Eq. (24), we obtain complex natural frequency as:

$$\Omega_{rn(1/2)}=\pm\sqrt{\lambda_{rn}-\nu_{rn}{}^2}+i\,\nu_{rn}=\pm\,\omega_{rn}+i\,\nu_{rn}, \tag{26}$$

where

$$\lambda_{rn}=\frac{\tilde{C}}{\tilde{A}}=\frac{\tilde{k}\Lambda+\eta h H_x^2\left(\alpha_r^2-\beta_n^2\right)\Lambda+\alpha_r^4D_{11}+\beta_n^4D_{22}+2\alpha_r^2\beta_n^2(D_{12}+2D_{66})}{\Lambda\left[\rho h+\sum_{j=1}^{s}\frac{4m_j}{ab}\sin^2(\alpha_r x_j)\sin^2\left(\beta_n y_j\right)\right]}, \tag{27a}$$

$$\nu_{rn}=\frac{\tilde{B}}{\tilde{A}}=\frac{\tilde{b}\Lambda+\tau_d\left(\alpha_r^4D_{11}+\beta_n^4D_{22}+2\alpha_r^2\beta_n^2(D_{12}+2D_{66})\right)}{2\Lambda\left[\rho h+\sum_{j=1}^{s}\frac{4m_j}{ab}\sin^2(\alpha_r x_j)\sin^2\left(\beta_n y_j\right)\right]}. \tag{27b}$$

or dimensionless form

$$\overline{\lambda}_{rn}=\frac{K\overline{\Lambda}+\mathrm{MP}\left(\overline{\alpha}_r^2-\overline{\beta}_n^2\right)\Lambda+\overline{\alpha}_r^4+R^4\beta_n^4Z_{22}+2\alpha_r^2R^2\beta_n^2(Z_{12}+2Z_{66})}{\overline{\Lambda}\left[1+\sum_{j=1}^{s}4\overline{m}_j\sin^2(\overline{\alpha}_r\overline{x}_j)\sin^2\left(\overline{\beta}_n\overline{y}_j\right)\right]}, \tag{27c}$$

$$\overline{\nu}_{rn}=\frac{B\overline{\Lambda}+T_d\left(\overline{\alpha}_r^4+R^4\beta_n^4Z_{22}+2\alpha_r^2R^2\beta_n^2(Z_{12}+2Z_{66})\right)}{2\overline{\Lambda}\left[1+\sum_{j=1}^{s}4\overline{m}_j\sin^2(\overline{\alpha}_r\overline{x}_j)\sin^2\left(\overline{\beta}_n\overline{y}_j\right)\right]}. \tag{27d}$$

in which dimensionless parameters are defined as:

$$\overline{\lambda}_{rn}=\lambda_{rn}a^2\sqrt{\frac{\rho h}{D_{11}}},\quad \overline{\nu}_{rn_{rn}}=\nu_{rn}a^2\sqrt{\frac{\rho h}{D_{11}}},\quad B=\tilde{b}\frac{a^2}{\sqrt{\rho h D_{11}}},$$

$$T_d=\tau_d\sqrt{\frac{D_{11}}{a^4\rho h}}$$

$$R=\frac{a}{b},\quad K=\tilde{k}\frac{a^4}{D_{11}},\quad \eta=\frac{\sqrt{\mu}}{a},\quad \overline{\alpha}_r=r\pi,\quad \overline{\beta}_n=n\pi,\quad \frac{D_{22}}{D_{11}}=Z_{22},$$
$$\frac{D_{12}}{D_{11}}=Z_{12},\quad \frac{D_{66}}{D_{11}}=Z_{66},\quad \overline{\Lambda}=1+\eta\left(\overline{\alpha}_r^2+R^2\overline{\beta}_n^2\right),\quad \mathrm{MP}=\frac{\eta h H_x^2 a^2}{D_{11}}. \tag{27e}$$

where the term λ_{rn} denotes squared value of the natural frequency. It should be noted that the real part of the complex natural frequency Eq. (26) represents the damped natural frequency ω_{rn}, while the imaginary part represents the damping ratio ν_{rn} of the viscoelastic orthotropic nanoplate.

Now, we can obtain new form of damped natural frequency as:

$$f_{rn}=\frac{\omega_{rn}}{2\pi}=\frac{\sqrt{\lambda_{rn}-\nu_{rn}{}^2}}{2\pi}. \tag{28}$$

By using the expression (28), we obtain the new form of damped natural frequency without influence of added mass of nanoparticles, magnetic field and external interaction from viscoelastic medium as:

$$f_{0,rn}=\frac{1}{2\pi}\left\{\frac{\alpha_r^4D_{11}+\beta_n^4D_{22}+2\alpha_r^2\beta_n^2(D_{12}+2D_{66})}{\Lambda\rho h}-\left[\frac{\tau_d\left(\alpha_r^4D_{11}+\beta_n^4D_{22}+2\alpha_r^2\beta_n^2(D_{12}+2D_{66})\right)}{\Lambda\rho h}\right]^2\right\}^{1/2} \tag{29}$$

Finally we define damped frequency shift of the sensor in the following form

$$\Delta f_{rn}=f_{0,rn}-f_{rn}, \tag{30}$$

and relative damped frequency shift as:

$$\Phi_{rn}=\frac{\Delta f_{rn}}{f_{0,rn}}=\frac{f_{0,rn}-f_{rn}}{f_{0,rn}}. \tag{31}$$

In similar manner we define relative shift of damping ratio as

$$N_{rn}=\frac{\nu_{0,rn}-\nu_{rn}}{\nu_{0,rn}}. \tag{32a}$$

where $\nu_{0,rn}$ is damped ratio without the influence of added masses of nanoparticles and external interaction from viscoelastic medium defined as:

$$\nu_{0,rn}=\frac{\tau_d\left(\alpha_r^4D_{11}+\beta_n^4D_{22}+2\alpha_r^2\beta_n^2(D_{12}+2D_{66})\right)}{2\Lambda\rho h}. \tag{32b}$$

In the following analysis, we consider only the relative frequency shift and damped ratio shift for the first vibration mode i.e. for $r=1$ and $n=1$.

In general, the exact closed form solution for natural frequencies for the free vibration of nanoplates is not funded. However, for the case of simply supported nanoplate, the exact closed form solution for natural frequencies can be obtained. For other types of boundary conditions regarding to the clamped or free edges of nanoplate or any other combination, the exact solutions for natural frequencies cannot be obtained. In such cases, one can use some of the available numerical or approximation methods to calculate the frequencies. Adhikari and Chowdhury [6] and Murmu and Adhikari [21], proposed a method based on energy principle to find approximated values for natural frequencies of cantilever graphene sheet. In this work, we have shown an analytical procedure to obtain exact solutions for complex natural frequencies of the graphene sheets with attached nanoparticles utilizing the nonlocal theory of viscoelasticity.

4. Numerical results and validation study

In the first part of this section, the obtained analytical results are validated with the results from the literature. Introducing various simplifications in the expressions for complex's natural frequency and damped shift frequency, we can obtain expressions that allow us to perform obvious comparisons between two separate results. However, in detailed parametric study we have shown several numerical examples that explains the influence of different physical and geometrical properties i.e. parameters of the system on dynamical behavior of mass-nanosensor.

4.1. Analytical validation study

The authors did not find any similar study analyzing the problem of nonlocal damped vibration of SLGS with attached masses that is affected by in-plane magnetic field and used for mass-sensing application. Nevertheless, by reducing derived expressions for damped natural frequency and damped frequency shift we can obtain results for already presented models of mass-nanosensors based on vibration of SLGS. Therefore, in this subsection we present several analytical studies for natural frequencies and frequency shifts to verify the obtained analytical results of magnetically affected mass-nanosensor. It should be noted that the authors have found two corresponding works in which vibration analysis of SLGS for mass-nanosensor application is presented by Shen et al. [22] and Fazelzadeh and Ghavanloo [24]. Now, we introduce some simplifications in Eqs. (28) and (30) and reduce expressions for damped natural frequency and damped shift frequency as follow. When the parameters of stiffness $\tilde{k}$ and viscosity $\tilde{b}$ of foundation, magnetic field parameter $H_x$and internal viscosity τ_d are equal to zero, we obtain reduced equation for resonant frequency and frequency shift as:

$$f_{rn}=\frac{\omega_{rn}}{2\pi}=\frac{1}{2\pi}\left[\frac{\alpha_r^4D_{11}+\beta_n^4D_{22}+2\alpha_r^2\beta_n^2(D_{12}+2D_{66})}{\Lambda\left[\rho h+\sum_{j=1}^{s}\frac{4m_j}{ab}\sin^2(\alpha_r x_j)\sin^2\left(\beta_n y_j\right)\right]}\right]^{1/2}, \tag{33}$$

and

$$\Delta f_{rn}=f_{0,rn}-f_{rn}=\frac{1}{2\pi}\left[\frac{\alpha_r^4D_{11}+\beta_n^4D_{22}+2\alpha_r^2\beta_n^2(D_{12}+2D_{66})}{\Lambda\rho h}\right]^{1/2}-\frac{1}{2\pi}\left[\frac{\alpha_r^4D_{11}+\beta_n^4D_{22}+2\alpha_r^2\beta_n^2(D_{12}+2D_{66})}{\Lambda\left[\rho h+\sum_{j=1}^{s}\frac{4m_j}{ab}\sin^2(\alpha_r x_j)\sin^2\left(\beta_n y_j\right)\right]}\right]^{\frac{1}{2}}. \tag{34}$$

From Eqs. (17) and (21) presented in the paper by Fazelzadeh and Ghavanloo [24], we can also obtain expressions (33) and (34) when the temperature change is equal to zero. In the following, we have reduced the expression for damped natural frequency of magnetically affected orthotropic viscoelastic nanoplate (Eq. (28)) and damped frequency shift (Eq. (30)). That simplifications yields the case of isotropic nanoplate system by introducing the following parameters $E_1=E_2=E$, $\vartheta_{12}=\vartheta_{21}=\vartheta$ and $G_{12}=G$ which leads to the new bending stiffness $D_{11}=D_{22}=(D_{12}+2D_{66})=D$ and parameters of external influences $H_x=\tau_d=\tilde{k}=\tilde{b}=0$ and $j=1$ in Eq. (28), where we obtain natural frequency of the form

$$f_{rn}=\frac{\omega_{rn}}{2\pi}=\frac{1}{2\pi}\left[\frac{D\left(\alpha_r^2+\beta_n^2\right)^2}{\Lambda\left[\rho h+\frac{4m_1}{ab}\sin^2(\alpha_r x_j)\sin^2\left(\beta_n y_j\right)\right]}\right]^{1/2}. \tag{35}$$

This equation is the same as Eq. (25) from the paper by Shen et al. [22]. In order to justify our analytical results for damped

natural frequency, by searching the literature we have found the paper where the authors studied the free vibration of viscoelastic orthotropic nanoplate, see [29]. By neglecting the effects of magnetic field parameter and attached mass of nanoparticles in Eq. (27) we obtain

$$\tilde{\lambda}_{rn}=\frac{k\Lambda+\alpha_r^4D_{11}+\beta_n^4D_{22}+2\alpha_r^2\beta_n^2(D_{12}+2D_{66})}{\Lambda\rho h}, \tag{36a}$$

$$\tilde{\nu}_{rn}=\frac{b\Lambda+\tau_d\left(\alpha_r^4D_{11}+\beta_n^4D_{22}+2\alpha_r^2\beta_n^2(D_{12}+2D_{66})\right)}{2\Lambda\rho h}. \tag{36b}$$

or in dimensionless form as

$$\overline{\lambda}_{rn}=\frac{K\overline{\Lambda}+\overline{\alpha}_r^4+R^4\overline{\beta}_n^4Z_{22}+2\overline{\alpha}_r^2\overline{\beta}_n^2R^2(Z_{12}+2Z_{66})}{\overline{\Lambda}}$$

$$\Rightarrow\quad \omega=\sqrt{\overline{\lambda}_{rn}}, \tag{37a}$$

$$\overline{\nu}_{rn}=\frac{B\overline{\Lambda}+T_d\left(\overline{\alpha}_r^4+R^4\overline{\beta}_n^4Z_{22}+2\overline{\alpha}_r^2\overline{\beta}_n^2R^2(Z_{12}+2Z_{66})\right)}{2\overline{\Lambda}}$$

$$\Rightarrow\quad \xi=\frac{\overline{\nu}_{rn}}{\omega}, \tag{37b}$$

which are the expressions for dimensionless undamped frequency ω and damping ratio ξ (see Eq. (17) as in the paper by Pouresmaeeli et al. [29]). From obtained results for damped natural frequencies and damped frequency shifts, we can conclude that the present study can be considered as the continuation study of previous works in the field of nanosensors. The extension presented here is the analysis of damped vibration of SLGS together with considered influence of magnetic field that are used for mass-nanosensor application.

4.2. Numerical examples

In Table 1, several typical examples of single and multiple added masses on the nanosensor are presented in order to examine the influence of magnetic field and damping on relative damped frequency shift Φ_{rn} and relative shift of damping ratio N_{rn}. In all of the examples, masses are located along the middle line of nanoplate. As for example, in [24] the authors have examined several cases by adding the masses in more arbitrary order. In this work, that is not the case since the used approach is sufficient to explain significant frequency shifts where multiple masses are added along the middle line of nanoplate. Higher number of point masses can represent some kind of biological particle, which is attached on nanoplate as distributed mass. The following values of parameters used in numerical examples are adopted from paper by Fazelzadeh and Ghavanloo [24]: length of nanoplate $a=9.519$ [nm], width $b=4.844$ [nm], elastic modules $E_1=2.434$ [TPa] and $E_2=2.473$ [TPa] of orthotropic nanoplate, shear modulus $G_{12}=1.039$ [TPa], Poisson's ratios $\vartheta_{12}=\vartheta_{21}=0.197$, thickness of nanoplate $h=0.129$ [nm] and mass density $\rho=6316$ [kg/m^3]. Parameters of the in-plane magnetic field, stiffness and damping coefficients of the viscoelastic medium are given in dimensionless form. In this paper, we adopted values of internal (structural) damping coefficient T_d in certain range in order to describe the influence of structural damping on dynamical behavior of the system [29]. Furthermore, influences of these parameters on relative damped frequency shifts are presented in four different cases where a number of masses and its locations on the nanoplate are distinct. In all cases, frequency shifts increases for an increase of the magnetic field parameter. When no internal damping and damping of the viscoelastic medium are considered, the relative damped frequency shift is higher. By taking into account and increasing the values of damping parameters and dimensionless stiffness of the medium, the value of relative damping frequency shift decreases. Such decrease of relative damped frequency shift is attributed to the damping that is introduced into the system, which leads to a decrease of damped complex natural frequency.

The effect of a single or multiple masses on frequency shift is also significant and depends of the appropriate location on the nanoplate. It is easy to note that frequency shift is significantly larger for a single mass located at the middle of the nanoplate compared to the system with two, four or nine masses located at the middle line of a nanoplate. This is attributed to the location of attached masses since the central position causes the largest frequency shift whereas the positions of masses towards boundary cause a smaller frequency shifts. In addition, an increase of a number of masses does not cause a significant increase of frequency shift that might be attributed to the symmetric positions of attached masses with respect to the center of nanoplate and their nearness to the boundaries of a nanoplate.

Fig. 2 shows the influence of nonlocal parameter on relative damped natural frequency and relative damping ratio shift for three different mass cases. From Fig. 2a) it can be noticed that an increase of nonlocal parameter is followed by an increase of relative damped frequency shift in all three mass cases. Further, the lowest frequency shift can be observed for the case with two masses, the larger shift is for the case with four masses and the largest one is for the single mass system. An opposite cases can be observed for the change of relative damping ratio shift, where an increase of nonlocal parameter causes a decrease of damping ratio shift, (Fig. 2b).

The influence of non-dimensional magnetic field parameter on relative damped frequency shift and relative damping ratio shift is shown in Fig. 3a). One can notice almost linear increase of frequency shift for an increase of nonlocal parameter. This is related to the well-known property of graphene nanostructures whose natural frequency increases for an increase of the magnitude of magnetic field that as discussed in a number of works. As expected, in Fig. 3b) it can be noticed that there is no influence of magnetic field on damping ratio shift due to the fact that it does not affect the damping properties of the system [40].

To examine the changes of relative damped frequency shift and relative damping ratio shift for changes of internal damping parameter we plotted several curves in Fig. 4 for nanosensor system with different number of masses. Change of damped frequency shift is weak for an increase of internal damping parameter. However, major changes can be observed for the damping ratio shift where an instant jump occurs in all three mass cases, for low values of damping parameter. After a sudden jump, the frequency shift curves slightly increases and stagnate for further increase of internal damping parameter.

In order to investigate the effect of different mass weights on the relative damped frequency shift and relative damping ratio shift we plotted Fig. 5 for different number of masses in the system. It is obvious that both relative frequency shift (Fig. 5a)) and relative damping ratio shift (Fig. 5b)) are increasing for an increase of mass weight. In spite overall weight of attached masses is equal in all cases i.e. when a single and multiple masses are considered, frequency and damping ratio shifts differs significantly in the case of multiple masses. The reason for this is the fact that overall added mass is distributed i.e. located at different positions on the nanosensor in the case of several masses that causes major changes in the dynamic behavior.

Finally, Fig. 6 shows the influence of the length-to-thickness ratio ψ on the relative damped frequency and damping ratio shift for different number of nanoparticles. It is obvious that frequency and damping ratio shifts are having extremal i.e. maximum values for a certain value of length-to-thickness ratio. The maximum values of shift imply the maximum sensibility that can be achieved for certain critical value of aspect ratio, which improves the

Table 1
The relative damped frequency shift for different values of magnetic field parameter, viscoelastic coefficients and numbers and positions of masses.

Mechanical model	$m=10$ [cg]	Position (ϑ_j,ζ_j)	Viscoelastic coefficients	Magnetic field parameter MP			
				MP = 0	MP = 10	MP = 25	MP = 50
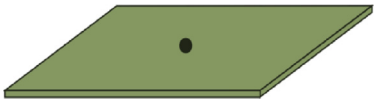	$m_1=m$	(0.5, 0.5)	$T_d=0$ $B=0$ $K=0$	[a]**0.304063**	0.37154	0.489205	0.806363
			$T_d=0.001$ $B=0.01$ $K=10$	0.301725	0.368979	0.486107	0.798545
			$T_d=0.005$ $B=0.01$ $K=10$	0.30005	0.367782	0.485845	0.803072
	$m_1=m/2$	(0.25, 0.5)	$T_d=0$ $B=0$ $K=0$	[a]**0.19217**	0.270496	0.407079	0.77523
			$T_d=0.001$ $B=0.01$ $K=10$	0.189482	0.267552	0.403519	0.766246
	$m_2=m/2$	(0.75, 0.5)	$T_d=0.005$ $B=0.01$ $K=10$	0.188167	0.266858	0.404071	0.773748
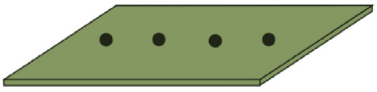	$m_1=m/4$	(0.2, 0.5)	$T_d=0$ $B=0$ $K=0$	[a]**0.225119**	0.300251	0.431263	0.784398
	$m_2=m/4$	(0.4, 0.5)	$T_d=0.001$ $B=0.01$ $K=10$	0.222534	0.297419	0.427837	0.775753
	$m_3=m/4$	(0.6, 0.5)					
	$m_4=m/4$	(0.8, 0.5)	$T_d=0.005$ $B=0.01$ $K=10$	0.221085	0.296546	0.428112	0.782279
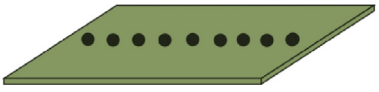	$m_1=m/9$	(0.1, 0.5) (0.2, 0.5) (0.3, 0.5) (0.4, 0.5) (0.5, 0.5) (0.6, 0.5) (0.7, 0.5) (0.8, 0.5)	$T_d=0$ $B=0$ $K=0$	[a]**0.207324**	0.284181	0.418201	0.779446
			$T_d=0.001$ $B=0.01$ $K=10$	0.204683	0.281288	0.414703	0.770618
	$m_2=m/9$	(0.9, 0.5)	$T_d=0.005$ $B=0.01$ $K=10$	0.203303	0.280509	0.415124	0.77766
	$m_3=m/9$ $m_4=m/9$ $m_5=m/9$ $m_6=m/9$ $m_7=m/9$ $m_8=m/9$ $m_9=m/9$						

[a] Values of relative shift frequency obtained by using Eq. (23) from paper Fazelzadeh and Ghavanloo [24].

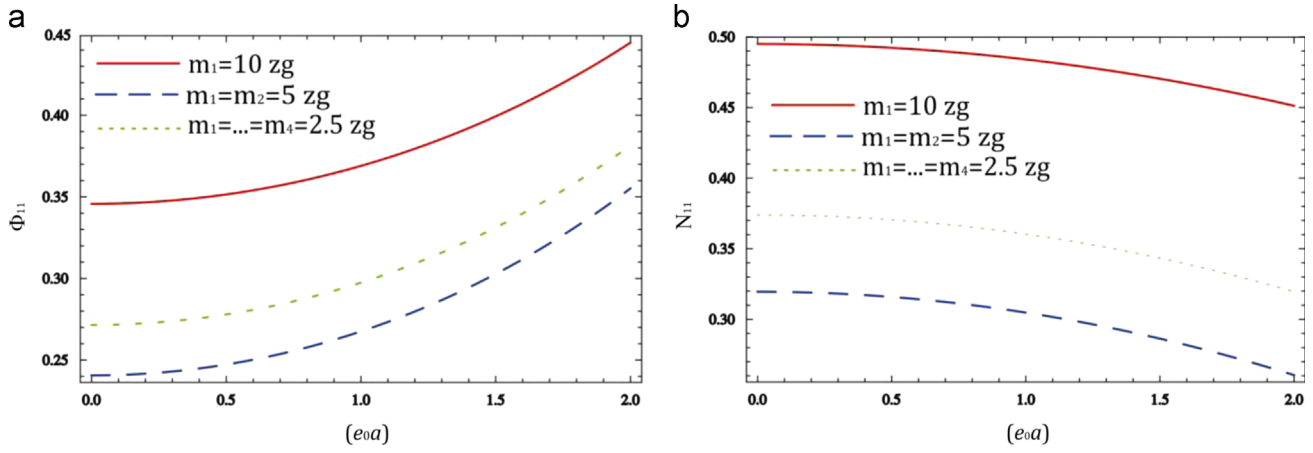

Fig. 2. Effects of nonlocal parameters on the a) relative damped frequency shift and b) relative damped ratio shift for different number of nanoparticles when the total added mass weight is $m=10$ [zg].

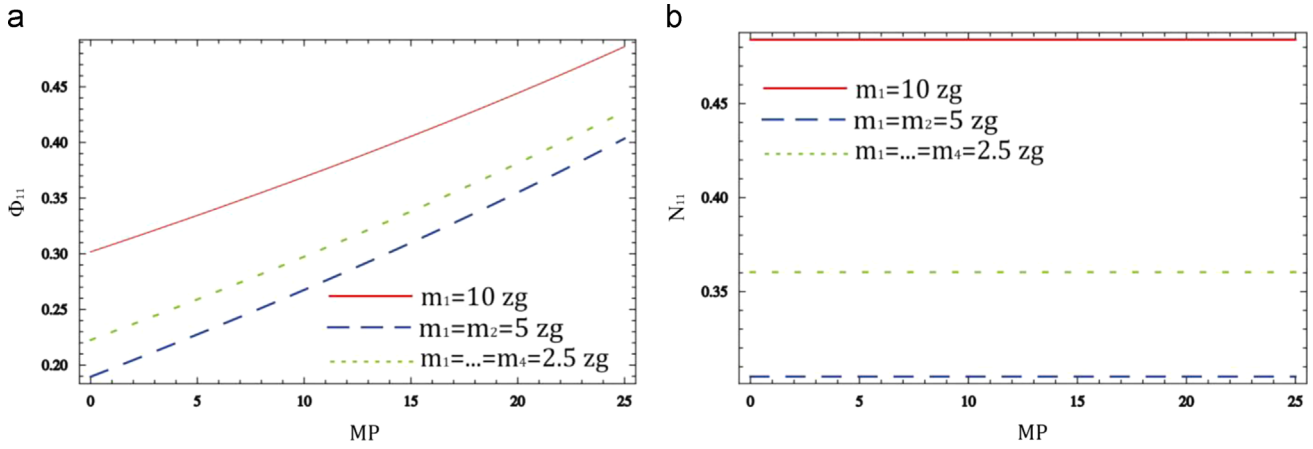

Fig. 3. Effects of in-plane magnetic field parameter on the (a) relative damped frequency shift and (b) relative damped ratio shift for different number of nanoparticles when the total added mass weight is $m = 10$ [zg].

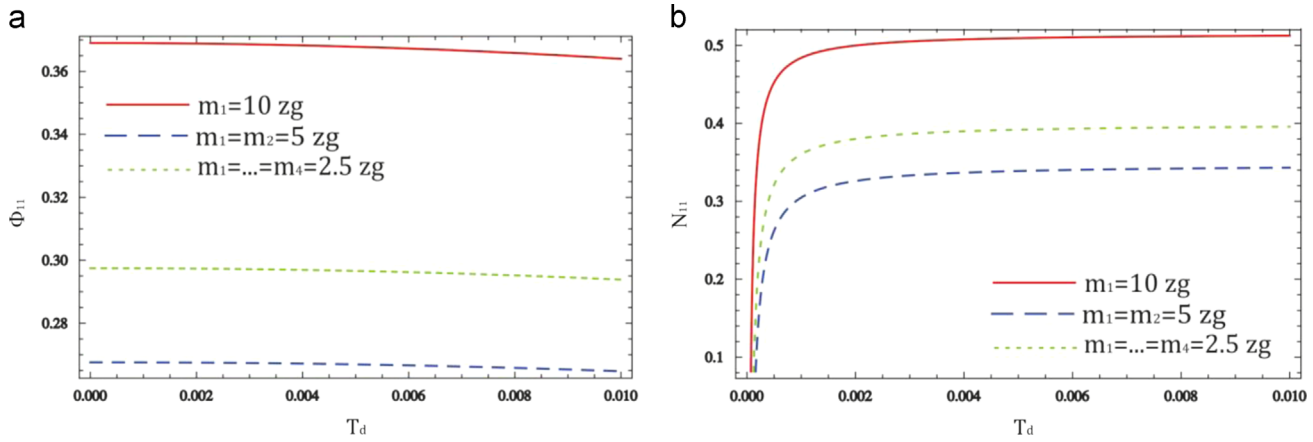

Fig. 4. Effects of internal damping parameter on the (a) relative damped frequency shift and (b) relative damped ratio shift for different number of nanoparticles when the total added mass weight is $m = 10$ [zg].

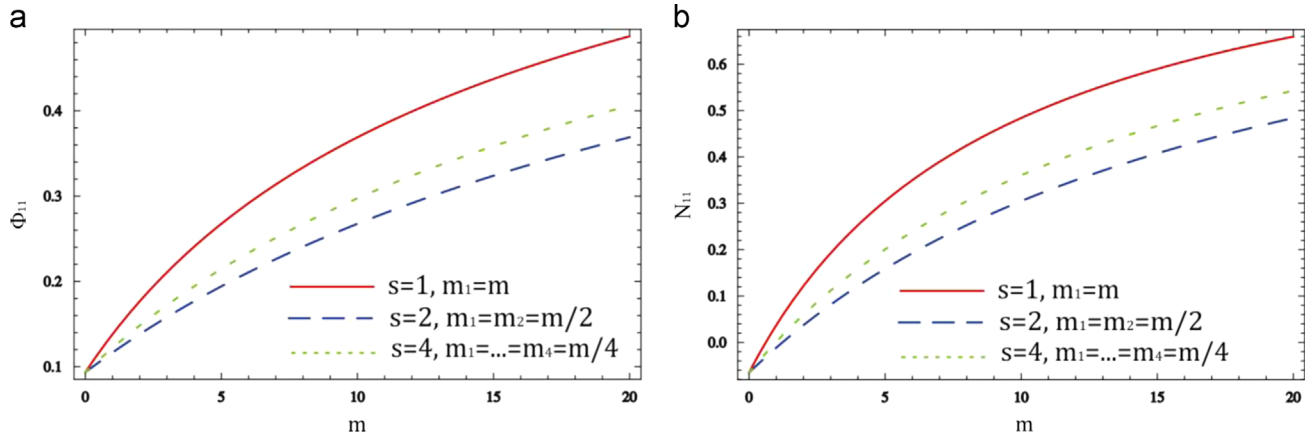

Fig. 5. Effects of total added mass weight on the (a) relative damped frequency shift and (b) relative damped ratio shift for different number of nanoparticles.

performances of mass-nanosensor. For the aspect ratio before the critical value, the frequency and damping ratio shifts increases and after the critical value, their values decreases for an increase of the aspect ratio. Moreover, this analysis shows that it is possible to find optimal dimensions of nanosensors in design process to achieve their maximal sensitivity properties.

Following the main idea to measure frequency shift in nanosensor devices for mass-sensing application, we investigated the case when the influence of magnetic field and vibration damping are considered. As it was observed in the numerical analysis, both effects are having significant influence on relative damped frequency shift and damping ratio shift. Damping slightly decreases

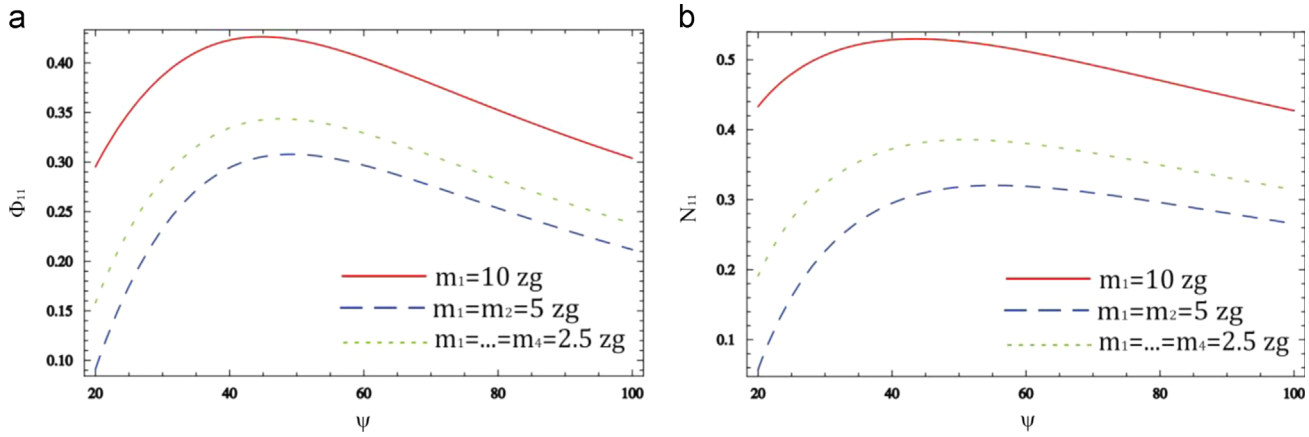

Fig. 6. Effects of length to thickness ratio $\psi = a/h$, on (a) relative damped frequency shift and (b) relative damped ratio shift, for different number of nanoparticles when the total added mass weight is $m = 10$ [zg].

the frequency shift caused by attached masses on nanosensor while magnetic field increases the frequency shift. Thus, in our theoretical prediction of damped frequency shifts we proved that magnetic field could be successfully applied to improve sensibility performances of mass-nanosensors besides the optimal value of length-to-thickness ratio. In addition, it should be noted that damping effects are having significant influence on dynamical behavior of nanomechanical systems and it needs to be considered for more accurate modeling [29,31].

5. Conclusion

Vibrating graphene sheets within a magnetic field are investigated for possible mass-nanosensor application. The mass-sensing is possible due to the shift of frequency from attached nanoparticles. An explicit relation for the relative damped frequency shifts and damping ratio shifts are derived based on the nonlocal theory and taking into account the effects of external magnetic field, internal damping and coefficients of the surrounding medium of the nanosensor. Validation study shows the accuracy and applicability of the obtained expressions, which represent a generalization of the previous works found in the literature. From the parametric study, one can notice that an increase of the magnitude of magnetic field causes an increase of frequency shift of nanosensor device and consequently increases its sensibility performances. On the other hand, considering damping properties of the nanosensor system it has been shown that it decreases the frequency shift and in such way decreases the sensibility properties of the system. Finally, we found that length-to-thickness ratio is having a significant influence on frequency and damping ratio shift. The main contributions of this work are:

(1) Closed form solution of damped natural frequency and damping ratio are obtained for viscoelastic orthotropic nanoplate with attached several nanoparticles;
(2) Relative damped frequency and damping ratio shifts are derived as functions of magnetic field parameter, internal damping coefficient and damping coefficient of viscoelastic medium;
(3) It is concluded that the external magnetic field has a large impact on the sensibility of mass-nanosensors;
(4) Optimal value of length-to-thickness ratio can be found in order to achieve the best sensibility of mass-nanosensor device.

Despite the proposed orthotropic nanoplate model catches much of the behavior of single-layer graphene sheet nanostructure and accounts for the magnetic field and damping effects, it has few limits that should be considered in future studies. Firstly, the presented model does not include van der Waals forces between nanoplate and attached nanoparticle. Secondly, additional investigations on frequency limits and the influence of chirality should be conducted. The results obtained in this paper can be used for further research on more complex graphene based nanosensor systems working in the presence of magnetic field.

Acknowledgments

This research was supported by the research grants of the Serbian Ministry of Education, Science and Technological Development under Numbers OI 174001, OI 174011 and TR 35006.

References

[1] Waggoner PS, Craighead HG. Micro-and nanomechanical sensors for environmental, chemical, and biological detection. Lab Chip 2007;7(10):1238–55.
[2] Calleja M, Kosaka PM, San Paulo Á, Tamayo J. Challenges for nanomechanical sensors in biological detection. Nanoscale 2012;4(16):4925–38.
[3] Sakhaee-Pour A, Ahmadian MT, Vafai A. Potential application of single-layered graphene sheet as strain sensor. Solid State Commun 2008;147(7):336–40.
[4] Chowdhury R, Adhikari S, Mitchell J. Vibrating carbon nanotube based biosensors. Phys E: Low-Dimens Syst Nanostruct 2009;42(2):104–9.
[5] Adhikari S, Chowdhury R. The calibration of carbon nanotube based bionanosensors. J Appl Phys 2010;107(12):124322.
[6] Adhikari S, Chowdhury R. Zeptogram sensing from gigahertz vibration: graphene based nanosensor. Phys E: Low-Dimens Syst Nanostruct 2012;44(7):1528–34.
[7] Eringen AC, Edelen DGB. On nonlocal elasticity. Int J Eng Sci 1972;10(3):233–48.
[8] Eringen AC. On differential-equations of nonlocal elasticity and solutions of screw dislocation and surface-waves. J Appl Phys 1983;54:4703–10.
[9] Peddieson J, Buchanan GR, McNitt RP. Application of nonlocal continuum models to nanotechnology. Int J Eng Sci 2003;41:305–12.
[10] Wang Q, Varadan VK, Quek ST. Small scale effect on elastic buckling of carbon nanotubes with nonlocal continuum models. Phys Lett A 2006;357:130–5.
[11] Reddy JN. Nonlocal theories for buckling bending and vibration of beams. Int J Eng Sci 2007;45:288–307.
[12] Pradhan SC, Phadikar JK. Small scale effect on vibration of embedded multilayered graphene sheets based on nonlocal continuum models. Phys Lett A 2009;373:1062–9.
[13] Murmu T, Adhikari S. Axial instability of double-nanobeam-systems. Phys Lett A 2011;375:601–8.
[14] Yang Y, Lim CW. A new nonlocal cylindrical shell model for axisymmetric wave propagation in carbon nanotubes. Adv Sci Lett 2011;4(1):121–31.
[15] Murmu T, Adhikari S. Nonlocal elasticity based vibration of initially prestressed coupled nanobeam systems. Eur J Mech A/Solids 2012;34:52–62.
[16] Huu-Tai T. A nonlocal beam theory for bending, buckling, and vibration of nanobeams. Int J Eng Sci 2012;52:56–64.

[17] Shen ZB, Sheng LP, Li XF, Tang GJ. Nonlocal Timoshenko beam theory for vibration of carbon nanotube-based mass-sensor. Physica E 2012;44:1169–75.
[18] Pouresmaeeli S, Fazelzadeh SA, Ghavanloo E. Exact solution for nonlocal vibration of double-orthotropic nanoplates embedded in elastic medium. Compos: Part B 2012;43:3384–90.
[19] Arani AG, Roudbari MA. Nonlocal piezoelectric surface effect on the vibration of Visco-Pasternak coupled boron nitride nanotube system under a moving nanoparticle. Thin Solid Films 2013;542:232–41.
[20] Murmu T, Adhikari S. Nonlocal frequency analysis of nanoscale mass-sensors. Sens Actuators A: Phys 2012;173(1):41–8.
[21] Murmu T, Adhikari S. Nonlocal mass nanosensors based on vibrating monolayer graphene sheets. Sens Actuators B: Chem 2013;188:1319–27.
[22] Shen ZB, Tang HL, Li DK, Tang GJ. Vibration of single-layered graphene sheet-based nanomechanical sensor via nonlocal Kirchhoff plate theory. Comput Mater Sci 2012;61:200–5.
[23] Wang K, Wang B. Vibration modeling of carbon-nanotube-based biosensors incorporating thermal and nonlocal effects *J Vib Control* 2014 1077546314534718, first published on July 4, http://dx.doi.org/10.1177/1077546314534718.
[24] Fazelzadeh SA, Ghavanloo E. Nanoscale mass sensing based on vibration of single-layered graphene sheet in thermal environments. Acta Mech Sin 2014;30(1):84–91.
[25] Kiani K. Magnetically affected single-walled carbon nanotubes as nanosensors. Mech Res Commun 2014;60:33–9.
[26] Su Y, Wei H, Gao R, Yang Z, Zhang J, Zhong Z, Zhang Y. Exceptional negative thermal expansion and viscoelastic properties of graphene oxide paper. Carbon 2012;50:2804–9.
[27] Ghorbanpour Arani A, Roudbari MA. Nonlocal piezoelastic surface effect on the vibration of Visco-Pasternak coupled boron nitride nanotube system under a moving nanoparticle. Thin Solid Films 2013;542:232–41.
[28] Lei Y, Adhikari S, Frishwell MI. Vibration of nonlocal Kelvin–Voigt viscoelastic damped Timoshenko beams. Int J Eng Sci 2013;66-67:1–13.
[29] Pouresmaeeli S, Ghavanloo E, Fazelzadeh SA. Vibration analysis of viscoelastic orthotropic nanoplates resting on viscoelastic medium. Compos Struct 2013;96:405–10.
[30] Lei Y, Murmu T, Adhikari S, Friswell MI. Dynamic characteristics of damped viscoelastic nonlocal Euler–Bernoulli beams. Eur J Mech A/Solids 2013;42:125–36.
[31] Imboden M, Mohanty P. Dissipation in nanoelectromechanical systems. Phys Rep 2014;534(3):89–146.
[32] Croy A, Midtvedt D, Isacsson A, Kinaret JM. Nonlinear damping in graphene resonators. Phys Rev B 2012;86(23):235435.
[33] Eichler A, Moser J, Chaste J, Zdrojek M, Wilson-Rae I, Bachtold A. Nonlinear damping in mechanical resonators made from carbon nanotubes and graphene. Nat Nanotechnol 2011;6(6):339–42.
[34] Karličić D, Kozić P, Pavlović R. Free transverse vibration of nonlocal viscoelastic orthotropic multi-nanoplate system (MNPS) embedded in a viscoelastic medium. Compos Struct 2014;115:89–99.
[35] Murmu T, McCarthy MA, Adhikari S. Vibration response of double-walled carbon nanotubes subjected to an externally applied longitudinal magnetic field: a nonlocal elasticity approach. J Sound Vib 2012;331:5069–86.
[36] Murmu T, McCarthy MA, Adhikari S. Nonlocal elasticity based magnetic field affected vibration response of double single-walled carbon nanotube systems. J Appl Phys 2012;111:113511.
[37] Narendar S, Gupta SS, Gopalakrishnan S. Wave propagation in single-walled carbon nanotube under longitudinal magnetic field using nonlocal Euler–Bernoulli beam theory. Appl Math Model 2012;36(9):4529–38.
[38] Gopalakrishnan S, Narendar S. Wave propagation in nanostructures. Switzerland, Springer; 2013.
[39] Wang H, Dong K, Men F, Yan YJ, Wang X. Influences of longitudinal magnetic field on wave propagation in carbon nanotubes embedded in elastic matrix. Appl Math Model 2010;34(4):878–89.
[40] Karličić D, Murmu T, Cajić M, Kozić P, Adhikari S. Dynamics of multiple viscoelastic carbon nanotube based nanocomposites with axial magnetic field. J Appl Phys 2014;115(23):234303.
[41] Li S, Xie HJ, Wang X. Dynamic characteristics of multi-walled carbon nanotubes under a transverse magnetic field. Bull Mater Sci 2011;34(1):45–52.
[42] Kiani K. Free vibration of conducting nanoplates exposed to unidirectional in-plane magnetic fields using nonlocal shear deformable plate theories. Phys E: Low-Dimens Syst Nanostruct 2014;57:179–92.
[43] Kiani K, Ghaffari H, Mehri B. Application of elastically supported single-walled carbon nanotubes for sensing arbitrarily attached nano-objects. Curr Appl Phys 2013;13(1):107–20.
[46] Kiani K. Transverse wave propagation in elastically confined single-walled carbon nanotubes subjected to longitudinal magnetic fields using nonlocal elasticity models. Phys E: Low-Dimens Syst Nanostruct 2012;45:86–96.
[47] Wang X, Shen JX, Liu Y, Shen GG, Lu G. Rigorous van der Waals effect on vibration characteristics of multi-walled carbon nanotubes under a transverse magnetic field. Appl Math Model 2012;36(2):648–56.
[48] Kiani K. Characterization of free vibration of elastically supported double-walled carbon nanotubes subjected to a longitudinally varying magnetic field. Acta Mech 2013;224(12):3139–51.
[49] Kiani K. Vibration and instability of a single-walled carbon nanotube in a three-dimensional magnetic field. J Phys Chem Solids 2014;75(1):15–22.
[50] Kiani K. Revisiting the free transverse vibration of embedded single-layer graphene sheets acted upon by an in-plane magnetic field. J Mech Sci Technol 2014;28(9):3511–6.
[51] Alibeigloo A. Free vibration analysis of nano-plate using three-dimensional theory of elasticity. Acta Mech 2011;222(1–2):149–59.
[52] Liu X, Wang F, Wu H. Anisotropic growth of buckling-driven wrinkles in graphene monolayer. Nanotechnology 2015;26(6):065701.
[53] Liu X, Wang F, Wu H. Anisotropic propagation and upper frequency limitation of terahertz waves in graphene. Appl Phys Lett 2013;103(7):071904.